XRD and XPS Study of Cu−Ni Interactions on Reduced Copper−Nickel−Aluminum Oxide Solid Solution Catalysts

A. R. Naghash, T. H. Etsell,* and S. Xu

Department of Chemical and Materials Engineering, 536 Chemical and Materials Engineering Building, University of Alberta, T6G 2G6, Edmonton, Alberta, Canada

Received August 24, 2005. Revised Manuscript Received January 17, 2006

Copper−nickel−aluminum oxide solid solutions were reduced in hydrogen to produce alumina-supported copper−nickel alloy catalysts. XRD patterns of reduced oxides showed that the type of active metals which emerged upon reduction were sensitive to the reduction temperature and the copper content. Variations from +0.8 to +1 eV were found in the experimental Ni $2p_{3/2}$ binding energy (BE) of nickel in the solid solutions compared to the experimental Ni $2p_{3/2}$ BE of bulk nickel, attributed to the Ni−Ni arrangements in the solid solution. Also, when the curve-fitted BE values of Ni $2p_{3/2}$ and Cu $2p_{3/2}$ of different reduced solid solutions were compared, it was found that copper and nickel were in different chemical states depending on reduction temperature and the amount of the copper. Changes in Ni $2p_{3/2}$ BE in the reduced solid solutions were also discussed in terms of the filling of nickel d-hole bands due to nickel−copper d−d band interactions. At both high copper content and reduction temperature, copper had a tendency to segregate in order to reduce the interfacial surface energies. This was postulated based on the observation that the Ni $2p_{3/2}$ curve-fitted BE values were restored to somewhat close to bulk nickel at a copper content of 11 mol % and reduction temperature of 700 °C.

Introduction

Direct thermal decomposition of light hydrocarbons, such as methane or ethane, via catalytic decomposition may be an alternative route for producing pure hydrogen. In this approach, carbon nanotubes are formed during the decomposition as a value-added byproduct which can have a variety of applications.[1−4] Supported nickel catalysts are commonly used in this reaction and their activity and deactivation patterns have been widely studied.[5−10] We have studied the effect of preparation parameters, such as solution pH and the amount of the copper, on the preparation of copper−nickel−aluminum hydrotalcite (HT)-like precipitates as the precursors of catalysts for the production of carbon nanotubes and hydrogen.[11] Some results were also given on the reducibility of calcined precipitates and the catalytic activity of alumina-supported copper-doped nickel catalysts but they were not comprehensive. In this paper we examine the structure and the nature of alumina-supported copper-doped nickel catalysts, produced from the reduction of the calcined precipitates of the type discussed in the previous work,[11] in a more detailed manner.

Nickel and copper both have fcc structures with lattice parameters of 3.51 and 3.61 Å and melting points of 1453 and 1083 °C, respectively.[12] They form a continuous solid solution of cupro-nickel binary alloys crystallized in a cubic close-packed lattice. Copper is inactive for hydro- and dehydrogenation reactions; thus, the activity patterns shown by the Ni−Cu alloy system in catalytic reactions are of great interest.

Some controversial results for Ni−Cu alloy catalysts have been reported. For example, the addition of copper to nickel foils significantly reduced the catalytic activity of styrene hydrogenation and hydrogenolysis of ethane to methane.[13,14] The decrease in catalytic activity was explained by changes in electronic properties of nickel upon the addition of copper.[13] On the other hand, for ethylene hydrogenation, it was found that addition of copper increased the catalytic activity above that of pristine nickel powder alone.[15−17] Due to these conflicting results, research on copper−nickel alloys was focused toward the surface of the alloy catalyst. The catalyst surface plays the main role in the catalytic reactions and the composition of the alloy surface may not be the same as the bulk due to differences in the volatility of nickel and copper.[18] Results of surface studies by ultraviolet photoelec-

* Corresponding author. Tel: (780) 492-5594. Fax: (780) 492-2881. E-mail: tom.etsell@ualberta.ca.

(1) Shah, N.; Panjala, D.; Huffman G. *Energy Fuels* **2001**, *15*, 1528.
(2) Li, Y.; Chen, J.; Qin Y.; Chang L. *Energy Fuels* **2000**, *14*, 1188.
(3) Rostrup-Nielson, J. R. In *Catalytic Steam Reforming Science and Engineering*; Anderson, J. R., Boudart, M., Eds.; Springer: Berlin, 1984; Vol. 5, p 124.
(4) Rostrup-Nielson, R. J. *Catal. Today* **1993**, *18*, 305.
(5) Choudhary, T. V.; Sivadinarayana, C.; Chusuei, C. C.; Klinghoffer, A.; Goodman D. W. *J. Catal.* **2001,** *199*, 9.
(6) Li, Y.; Chen, J.; Qin, Y.; Chang, L. *J. Catal.* **1998**, *178*, 76.
(7) Bernardo, C. A.; Alstrup, I.; Rostrup-Nielsen, J. R. *J. Catal.* **1985**, *96*, 517.
(8) Alzamora, L. E.; Ross Julian, R. H. *J. Chem. Soc., Faraday Trans.* **1981**, *77*, 665.
(9) Bartholomew, C. H. *J. Catal*. **1976**, *45*, 41.
(10) Robertson, S. D.; Kloet, S. C. *J. Catal.* **1975**, *39*, 234.
(11) Naghash, A. R.; Xu, Z.; Etsell, T. H. *Chem. Mater.* **2005**, *17*, 815.
(12) Votton, F. A.; Wilkinson, G. In *Advanced Inorganic Chemistry*, 2nd ed.; Wiley-Interscience: London, 1966.
(13) Khulbe, K. C.; Mann, R. S. *Catal. Rev. Sci. Eng.* **1982**, *24*, 311.
(14) Sinfelt, J. H.; Carter, J. L.; Yates, D. J. C. *J. Catal*. **1974**, *24*, 28.
(15) Best, R. J.; Russel, W. W. *J. Am. Chem. Soc*. **1954**, *76*, 838.
(16) Gharpurey, M. K.; Emmett, P. H. *J. Phys. Chem.* **1961**, *65*, 1182.
(17) Hall, W. K.; Emmett, P. H. *J. Chem. Phys.* **1958**, *62*, 816.

10.1021/cm051910o CCC: $33.50
Published on Web 04/15/2006

tron spectroscopy suggested that each Ni and Cu atom retained much of its atomic character.[19] The d band vacancies theory was also suggested to account for the BE changes of nickel and copper upon alloying in X-ray photoelectron spectroscopy (XPS) studies.[20] Moreover, it was recognized that, in addition to the d band vacancies theory, other factors, such as surface composition of alloys, must also be taken into account when the properties of nickel−copper alloy catalysts are investigated. Studies of hydrogen adsorption showed that the heat of adsorption decreases exponentially upon increasing the copper content according to the Arrhenius expression. However, no simple relationship was found between the heat of adsorption and the catalytic activity.[21]

In the case of supported copper−nickel alloy catalysts, a study on SiO_2 and $SiO_2-Al_2O_3$ supported copper−nickel catalysts prepared by impregnation showed that, at high nickel concentrations, a homogeneous solid solution of copper and nickel was formed, whereas at lower nickel concentrations, copper and nickel were separately aggregated.[22] Magnetostatic studies of 1−10 wt % nickel with copper on a silica support showed that the composition of the alloy particles was nonuniform, whereas a fairly homogeneous supported copper−nickel alloy was obtained by using relatively high nickel loadings where there was an increased oxide miscibility prior to reduction.[10] Despite numerous studies made on unsupported copper−nickel alloys and supported copper−nickel alloys prepared by impregnation, there has been relatively little work done on supported copper−nickel catalysts prepared by coprecipitation methods. The catalytic activity of unsupported copper−nickel alloy catalysts or supported copper−nickel catalysts produced by an impregnation method may be different from that of copper−nickel alloy catalysts produced by a coprecipitation method. The former catalysts are formed by impregnation and subsequent reduction of separate metal salts on the support, whereas the latter catalysts are formed by the reduction of homogeneous oxide solid solutions.

The preparation and characterization of copper−aluminum−nickel HT-like precipitates prepared by coprecipitation and their subsequent calcination to obtain copper−nickel−aluminum oxide solid solutions has been reported.[11] A temperature-programmed reduction (TPR) study of the oxide solid solutions was also presented. In this work, results concerning X-ray diffraction (XRD), X-ray photoelectron spectroscopy (XPS), and Auger imaging studies of reduced copper−nickel−aluminum oxide solid solutions are reported. The aim of XRD analysis was to determine the type of metal phases which formed upon reduction of oxide solid solutions in a reducing atmosphere (hydrogen) as well as to reveal any Cu−Ni−Al synergism. The XPS studies revealed the chemical state of nickel, copper, and aluminum upon reduction as well as changes in the electronic properties of nickel in the presence of copper and aluminum. The Auger imaging studies revealed the copper and nickel distribution on the support surface. A model for the formation of alumina-supported copper-doped nickel catalysts was proposed based on these results.

Experimental Section

Preparation. The method for the preparation of the precipitates which gave rise to a material with an HT-like layer structure was described in detail in a previous paper.[11] In brief, the preparation was carried out by adding Na_2CO_3 solution as a pH modifier to a nitrate solution to keep the solution at a predetermined pH value of 7. The precipitates were washed carefully to remove Na^+ and NO_3^-. The cleaned precipitates were then dried under vacuum at 60 °C overnight followed by calcining in air in a quartz tube placed in a Thermolyne F-21125 furnace. Calcination was carried out at 270 °C for 17 h followed by 450 °C for 2 h. TPR was used to activate the oxide solid solution catalysts at temperatures ranging from 270 to 700 °C for different periods of time. In each test, 80 mg of oxide catalyst was reduced under a H_2 and N_2 gas mixture environment. The H_2 to N_2 volumetric ratio was fixed at 1:2 with a total gas flow of 27.5 mL min^{-1} (STP).

Characterization. X-ray diffraction patterns were obtained on a Philips diffractometer equipped with a PW1050/70 vertical goniometer and PW1370/10 X-ray generator using Cu Kα as the radiation source. The diffraction patterns were recorded over a 2θ range from 10 to 80° at a step size of 0.05°. The crystallographic parameters (d spacing, full-width at half-maximum (fwhm), unit cell parameter) were obtained from XRD data points, using PowerX software. The crystalline size of reduced samples was calculated form the Scherrer formula: $D(hkl)\ (\mathrm{nm}) = K\lambda/(\beta \cos(\theta_{hkl})$, where $\lambda_{(\mathrm{Cu\ K}\alpha)} = 0.15405$ nm, $\beta =$ fwhm (rad), $\theta_{(hkl)} =$ Bragg angle (°), and $K =$ instrumental factor, assuming that the crystallographic coherent domain of the particle is limited by its size.

Room-temperature XPS experiments were conducted using a Kratos Axis Ultra spectrometer with monochromatized Al Kα ($h\upsilon = 1486.71$ eV). The spectrometer was calibrated by the binding energy (84.0 eV) of Au $4f_{7/2}$ with reference to the Fermi level. The pressure in the analysis chamber during experiments was less than 5×10^{-10} Torr. A hemispherical electron-energy analyzer working at a pass energy of 20 eV was used to collect core-level spectra. The samples were mounted on a conductive carbon tape held in a copper sample holder and transferred directly into the analysis chamber. Charge effects were corrected by using the C 1s peak at 284.8 eV. A linear or Shirley background was applied to subtract the inelastic background of core-level peaks. Nonlinear optimization using the Marquardta algorithm was used to determine the peak model parameters such as peak positions, widths, and peak intensities. The model peak to describe XPS core-level lines for curve fitting was a product of Gaussian and Lorentzian functions.

The scanning electron microscopy (SEM) and Auger measurements were carried out using a JAMP-9500F JEOL Auger microprobe. The instrument was equipped with a Schottky field emitter. The accelerating voltage and emission current for SEM and Auger imaging were 25 kV and 10 nA, respectively. The sample was rotated 30° away from the primary electron beam to face the electron energy analyzer. The Auger peaks of Ni LMM (707 eV) and Cu LMM (916 eV) were selected for the mapping. The reason for choosing the Ni Auger electron spectroscopy (AES) peak at 707 eV rather than 844 eV was because the latter peak overlaps with Cu LMM peaks. The intensity of each pixel in the Auger imaging was calculated by $(P - B)/B$, where P and B are the peak and background intensities, respectively. Such intensity definition

(18) Sachtler, W. M. H.; Dorgelo, G. J. H.; Jongepier, R. *J. Catal.* **1965**, *4*, 100.
(19) Takeuchi, T.; Takayasu, O.; Tanada, S. *J. Catal.* **1978**, *54*, 197.
(20) Huffner, S.; Werthein, G. K.; Wernika, J. H. *Phys. Rev.* **1973**, *138*, 14511.
(21) Takasu, Y.; Matsuda, Y. *Electrochim. Acta* **1976**, *21*, 131.
(22) Swift, H. E.; Lutinski, F. E.; Kehl, W. L. *J. Phys. Chem.* **1965**, *69*, 3268.

Table 1. Summary of Preparation Conditions, Solid Phases Obtained after Calcination, and the Temperatures at Which Cu and Ni Cations Were Reduced for Different Cu−Ni−Al Oxide Solid Solutions

sample[a]	pH	x_{Al}	phases (XRD)	Cu^{2+} RT[b] (°C)	Ni^{2+} RT[b] (°C)
CuO			CuO	230	
NiO			NiO		430
A	7	0.25	NiO		500
B1.8	7	0.25	NiO		
B3.5	7	0.26	NiO	190	450
B11	7	0.24	NiO	176	415
B22	7	0.26	NiO		

[a] The sample code starting with letters A and B indicates synthesis without and with Cu doping, respectively. The suffix number reflects mole percentage of copper in reference to metallic elements used in synthesis. As an example, B3.5 represents a catalyst with 3.5 mol % Cu doped in 96.5 mol % nickel and aluminum. [b] Reduction temperature at which the maximum weight loss occurred.

helps to reduce the edge effect of islands and dots. An auto-probe tracking technique was used to compensate for possible drifting of the image during the analysis as a result of power instabilities.

Results and Discussion

TPR Study. It was determined that such copper, nickel, and aluminum HT-like precipitates at a (Ni + Cu)/Al mole ratio of 3 and Cu/Ni mole ratio in the range of 0.03−0.4 were isostructural with takovite ($Al_2Ni_6OH_{16}{\cdot}CO_3{\cdot}4H_2O$).[11] The calcination of precipitates resulted in homogeneous copper, nickel, and aluminum oxide solid solutions. Table 1 lists the catalysts examined in this paper. It shows for each sample the precipitation pH and the aluminum mole fraction, x_{Al} ($\cong$Al/(Ni + Cu + Al). The reduction temperatures of oxide samples at which the maximum weight loss occurred are also shown.

Based on the TPR results for reduction temperatures shown in Table 1 and discussed in previous work,[11] the following conclusions can be drawn:

(a) The reduction temperature of unsupported pristine CuO (230 °C) is substantially lower than unsupported pristine NiO (430 °C). This suggests that CuO was reduced more readily than NiO, in agreement with thermodynamics ($\Delta G°_f$ CuO $= -127$ kJ mol^{-1}, $\Delta G°_f$ NiO $= -216$ kJ mol^{-1}). This finding was important when the TPR results for copper- and aluminum-doped nickel catalysts were interpreted.

(b) For sample A (NiO containing 25 mol % Al), the temperature at which the maximum weight loss appeared (500 °C) is substantially higher than that for the reduction of unsupported pristine NiO (430 °C). This illustrates the greater stability of NiO in solid solution, such as catalyst A, than that of pristine NiO.[11] However, for samples B3.5 and B11, the temperatures at which the maximum weight losses occurred are attributed to the successive reduction of copper and nickel cations in the solid solutions. These reduction temperatures were shifted toward lower temperatures compared with unsupported pristine CuO and sample A, indicating that copper can markedly enhance the reducibility of mixed oxide catalysts.

XRD Study. To understand the nature of copper and nickel formed after the reduction of oxide solid solutions, the calcined B1.8, B3.5, and B11 precipitates were reduced at different temperatures. Subsequently, XRD tests were carried out on the reduced catalysts. Figures 1−3 show the XRD patterns of these samples (after a TPR at 270, 450, and 700 °C). Table 2 shows their crystallographic parameters obtained from the XRD data. For reference, the crystallographic parameters of NiO, Ni, and Cu are also shown in this table.[23] Fresh oxide catalyst was used each time the activation was carried out at a specific temperature. XRD patterns for sample B1.8 (1.8 mol % Cu) reduced at 270 and 450 °C (Figure 1a and b, respectively) showed three distinct diffraction peaks at $2\theta = 37°$, 44.3°, and 62.9°, which corresponded well with the three most intense peaks of NiO in JCPDS 78-0643. The lattice parameter a for sample B1.8, reduced at 270 and 450 °C (samples 1 and 2 in Table 2), also corresponded to that of nickel oxide. Although the reduction of Cu cations occurred at temperatures above 200 °C as was revealed by TPR results, the most intense copper peaks ($2\theta = 44.3°$, 50.4°, and 74.1°) in Figures 1a and 1b were not as visually prominent because copper contributes only 1.7% of the total weight for sample B1.8. When the activation temperature increased to 700 °C (Figure 1c), the XRD diffraction peaks corresponded well with the three most

Table 2. Crystallographic Parameters of the Cu−Ni−Al Oxide Solid Solutions Reduced at Different Temperatures

sample	copper content (mol %)	2θ (deg)	d (Å)	lattice parameter a (Å)	fwhm (deg)	crystalline size (nm)	RT[b] (°C)
NiO[a]		43.3	2.088	4.17			
Ni[a]		44.5	2.034	3.52			
Cu[a]		43.3	2.088	3.62			
1	1.8	43.0	2.088	4.20	1.30	7.5	270
2	1.8	43.3	2.074	4.17	1.35	7.1	450
3	1.8	44.3	2.047	3.54	0.80	11.9	700
4	3.5	43.0	2.088	4.20	1.80	5.3	270
5	3.5	43.4	2.087	3.60	1.60	6.0	450
6	3.5	44.2	2.042	3.55	0.85	11.2	700
7	11	44.2	2.047	3.55	1.55	6.1	270
8	11	44.1	2.051	3.56	1.55	6.1	450
9	11	44.4	2.038	3.53	0.85	11.2	700

[a] Obtained from ref 23. [b] Reduction temperature.

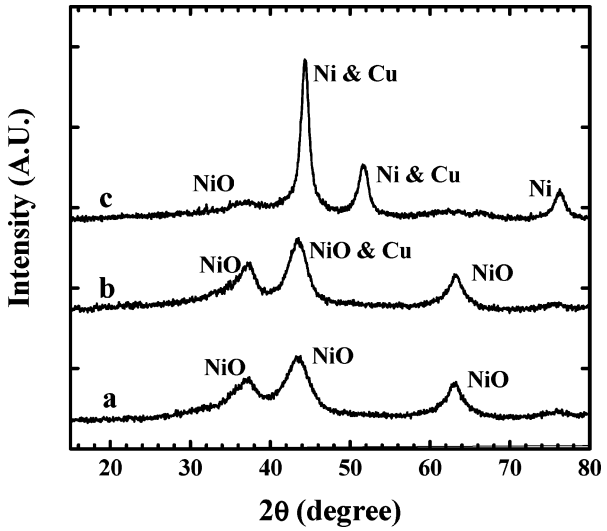

Figure 1. XRD patterns of sample B1.8 reduced at (a) 270 °C, (b) 450 °C, and (c) 700 °C.

(23) *XRD Diffraction Data*; Smith, J. V., Ed.; Am. Soc. Testing Mater., 1960; Vols. 1−5, Swarthmore, PA.

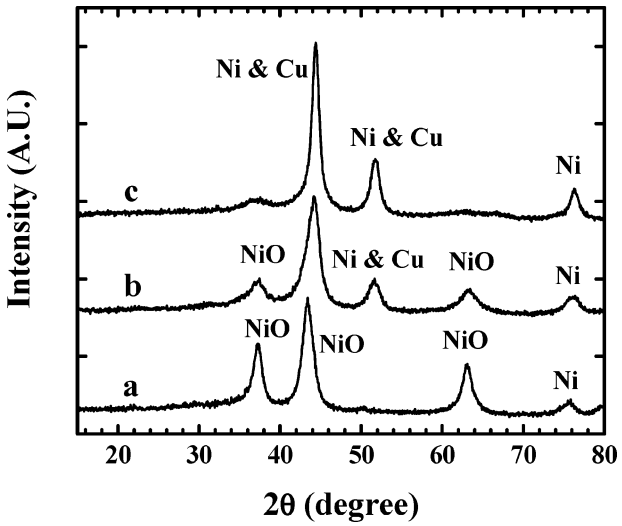

Figure 2. XRD patterns of sample B3.5 reduced at (a) 270 °C, (b) 450 °C, and (c) 700 °C.

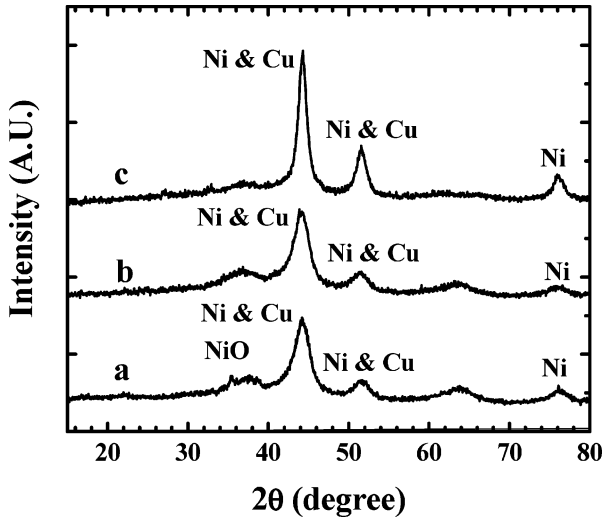

Figure 3. XRD patterns of sample B11 reduced at (a) 270 °C, (b) 450 °C, and (c) 700 °C.

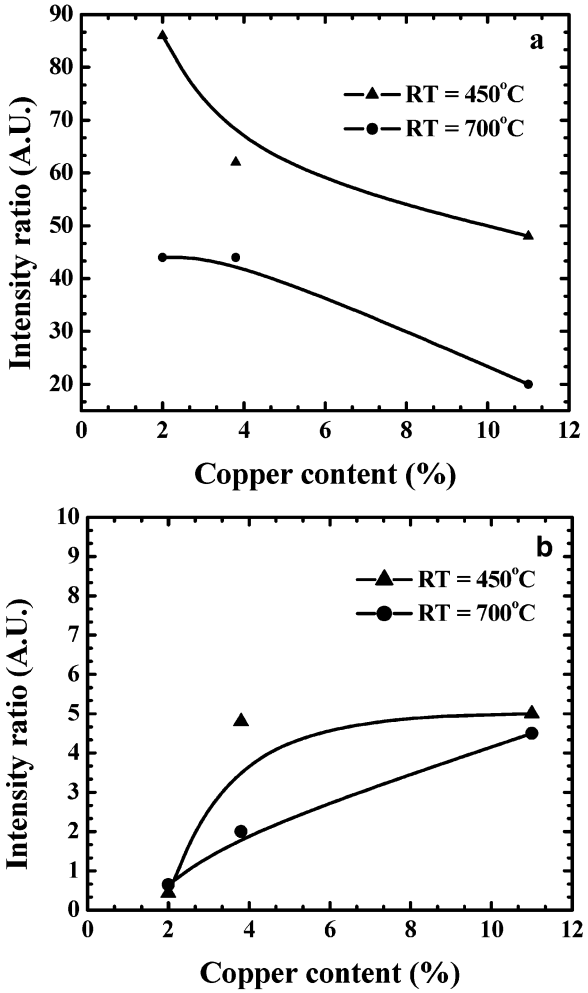

Figure 4. (a) XPS intensity ratios of Ni_{2p}/Al_{2p} as a function of copper content for samples B1.8, B3.5, and B11 reduced at different temperatures. (b) The XPS intensity ratios of Cu_{2p}/Al_{2p} as a function of copper content for samples B1.8, B3.5, and B11 reduced at different temperatures.

intense XRD peaks of Ni ($2\theta = 44.5°$, 51.8°, and 76.4°). In Table 2, the lattice parameter *a* for this sample (sample 3) is slightly higher (3.54 Å) than that of the reference nickel (3.52 Å). This is most likely due to the incorporation of copper, which has a larger lattice parameter (3.62 Å), into the nickel lattice.

For sample B3.5 (3.5 mol % Cu) reduced at 270 °C in Figure 2a, the XRD patterns resembled that of Figure 1a. However, when the temperature increased to 450 °C (Figure 2b), two major changes occurred: (i) the intensity of NiO peaks was reduced; (ii) in contrast to Figure 1b, XRD peaks of Ni were detected. This clearly indicates that when the copper content is increased from 1.8 to 3.5 mol %, the nickel cations can be reduced at lower temperatures. Although the wt % of copper increased to 3.4 for sample B3.5, its presence still could not be confirmed by its prominent diffraction peaks because of their proximity to the three prominent peaks of nickel. When the temperature was increased to 700 °C, all the XRD peaks (Figure 2c) matched those of nickel.

As the amount of copper increased to 11 mol % in sample B11, nickel XRD peaks appeared at 270 °C (Figure 3a), in contrast to samples B1.8 and B3.5, which indicates that the reduction temperature of nickel can be lowered further by increasing the amount of copper in the solid solution. When the reduction temperature was increased to 450 °C, the intensity of NiO peaks decreased while those of Ni peaks increased. The nickel lattice parameter also increased slightly to 3.56 Å for sample 8 from 3.55 Å for sample 7 in Table 2. At the activation temperature of 700 °C, however, the nickel lattice parameter decreased to 3.53 Å. It is assumed that, at the reduction temperature of 700 °C, at which most of the copper cations in sample B11 were reduced, copper segregation occurred for this sample.

XPS Study. The use of XPS intensity ratios of metal catalysts to that of the support provides information regarding the dispersion degree of the catalyst metal on the support.[24] Low concentrations of the active metals lead to lower relative XPS intensities and well-dispersed supported catalysts.

The results of the XPS intensity ratios of M/Al (M = Cu, Ni) as a function of copper content are shown in Figure 4. As shown in Figure 4a, the dispersion degree of nickel increased because the relative intensities of $Ni_{2p3/2}$ for samples

(24) Espinos, J. P.; Morales, J.; Barranco, A.; Caballero, A.; Holgado, J. P.; Conzalez-Elipe, A. R. *J. Phys. Chem. B* **2002**, *106*, 6921.

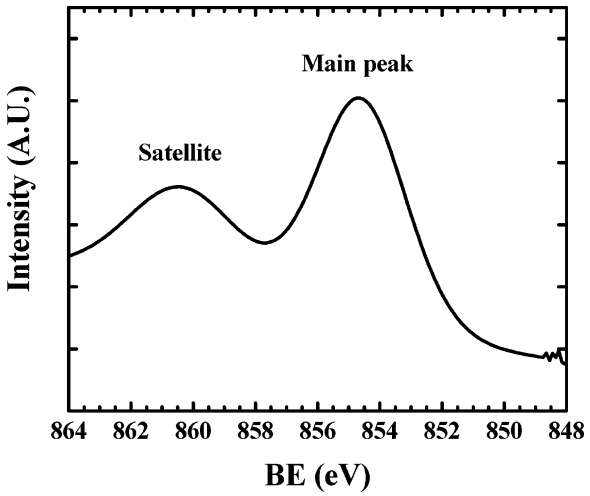

Figure 5. As-received bulk Ni $2p_{3/2}$ XPS spectrum.

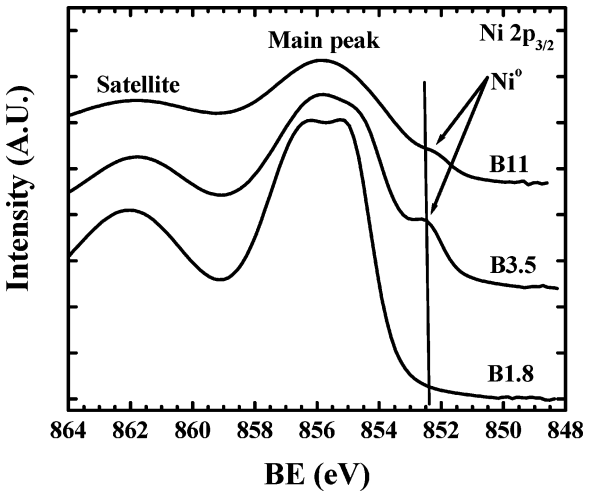

Figure 7. Ni $2p_{3/2}$ XPS spectra of samples B1.8, B3.5, and B11 reduced at 450 °C.

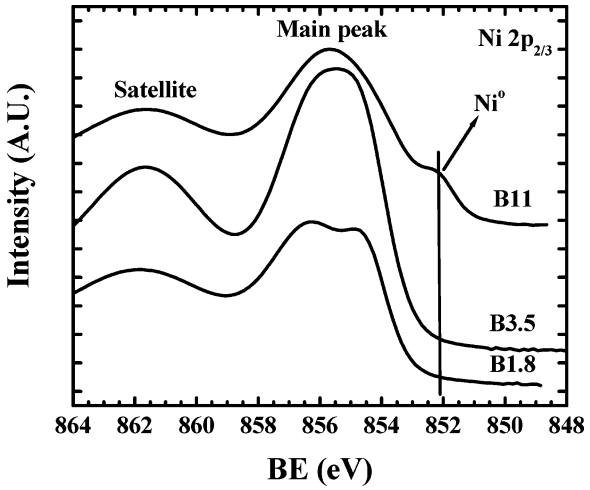

Figure 6. Ni $2p_{3/2}$ XPS spectra of samples B1.8, B3.5, and B11 reduced at 270 °C.

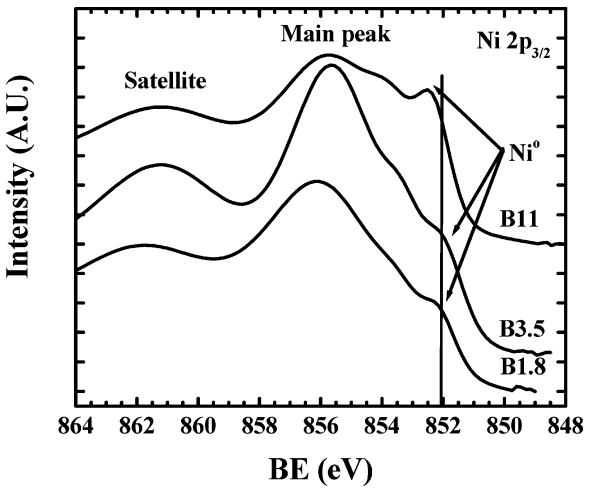

Figure 8. Ni $2p_{3/2}$ XPS spectra of samples B1.8, B3.5, and B11 reduced at 700 °C.

B1.8, B3.5, and B11 decreased as the amount of copper increased (decrease in the amount of the nickel). In contrast to nickel, the dispersion degree of copper decreased as its concentration increased. This is clearly illustrated by the diagram in Figure 4b, showing the evolution of the relative intensities of $Cu_{2p3/2}$ for samples B1.8, B3.5, and B11.

Figure 5 shows the Ni $2p_{3/2}$ XPS spectrum of as-received Ni. A series of Ni $2p_{3/2}$ XPS spectra for samples B1.8, B3.5, and B11, which were reduced at the same temperatures as those for XRD tests, are shown in Figures 6−8, respectively. Table 3 shows the experimental binding energies (BE), the binding energy values obtained from curve fitting of the experimental spectra, and the percentage of XPS peak intensities of copper, nickel, and oxygen contained in the samples.

The Ni $2p_{3/2}$ spectra for samples B1.8, B3.5, and B11 reduced at 270 °C (Figure 6) are characterized by a main peak with a satellite at higher BE. Ni can be interpreted similar to that previously reported for copper by Van der Laan et al. and cobalt by Fierro et al.[25,26] For divalent cobalt compounds the main peak corresponded to the final state $2p^5\ 3d^8$ L (L means a ligand hole) and the satellite peak to a $2p^5\ 3d^7$ final state. When the same concept is applied to nickel, the $2p^5\ 3d^9$ L and $2p^5\ 3d^8$ L notation could be assigned to the main and satellite peaks, respectively.

When Figures 5 and 6 are compared, the experimental Ni $2p_{3/2}$ XPS spectra of the main peak for samples B1.8, B3.5, and B11 solid solutions appeared at higher BEs than the BE of the main peak of the Ni $2p_{3/2}$ XPS spectrum for bulk Ni (+0.8 to +1 eV, as shown for samples 1, 2, and 3 in Table 3). A few other attributes could also be observed in the XPS spectra in Figure 6. First, for sample B1.8, the spectrum of the main peak showed two overlapped BE peaks at a low (854.5 eV) and a high (856.2 eV). This can account for changes with linking arrangements of Ni cations within the lattice in the oxide solid solution.[24] Thus, Ni^{2+} ions surrounded by Al^{3+} ions (through O^{2-} linkage) as the second neighbors showed a peak at higher BE than for isolated Ni^{2+} ions surrounded by other Ni^{2+} cations. In fact, the peak value at low BE (854.5 eV) for sample 1 (B1.8) in Table 3 is very close to the BE of bulk Ni (854.9 eV). Second, shape changes in XPS spectra were observed on going from sample B1.8

(25) Van der Laan, G.; Vestra, C.; Haas, C.; Sawatzky, G. A. *Phys. Rev.* **1981**, *23*, 4369.
(26) Fierro, G.; Jacono, M.; Lo Inversi, M.; Dragone, R.; Porta, P. *Top. Catal.* **2000**, *10*, 39.

Table 3. XPS Experimental Binding Energies, Binding Energies Obtained from Curve-Fitted Values of Experimental Spectra (Shown in First Set of Parentheses), and the Percentage of Peak Intensities (Shown in Second Set of Parentheses) for Cu−Ni−Al Oxide Solid Solutions Reduced at Different Temperatures

no.	sample	C 1s	Cu $2p_{3/2}$	Ni $2p_{3/2}$	O 1s	Al 2p	RT[a] (°C)
	Ni	284.0		854.9	531.5 (529.5, 531.5)		
1	B1.8	283.8	933.1 (933.1, 935.5) (65.9, 34.1)	855.6 (854.5, 856.2) (10.7, 89.3)	530.2 (530.0, 531.4) (34.1, 65.8)	74.0	270
2	B3.5	283.7	933.2 (932.6, 933.8) (56.7, 43.3)	855.6 (854.5, 856.0) (12.1, 87.9)	520.6 (529.7, 530.4) (45.0, 55.0)	73.7	270
3	B11	284.0	933.5 (932.1, 933.5) (57.5, 52.5)	855.7 (852.1, 854.0, 855.8) (3.2, 47, 49.8)	530.9 (529.8, 531.2) (20.0, 80.0)	74.0	270
4	B1.8	283.4	933.1 (932.9, 933.4) (17.5, 82.4)	855.8 (854.8, 856.3) (9.7, 90.3)	530.9 (530.4, 531.5) (68.3, 31.7)	74.2	450
5	B3.5	283.5	933.0 (932.0, 932.9) (24.9, 75.1)	855.6 (852.4, 854.4, 855.8) (9.7, 42.7, 47.5)	530.8 (530.1, 531.4) (34.8, 65.2)	74.2	450
6	B11	283.9	932.8 (932.1, 933.7) (33.2, 66.8)	855.8 (852.1, 854.1, 855.9) (9.2, 48.5, 42.3)	531.0 (530.8, 531.4) (33.8, 66.2)	74.0	450
7	B1.8	283.5	932.0 (931.8, 934.2) (68.2, 31.8)	856.1 (852.1, 853.4, 855.9) (55.6, 36.4, 8.0)	531.4 (529.3, 531.4) (5.2, 94.8)	74.4	700
8	B3.5	284.0	932.0 (931.8, 933.4) (84.9, 15.1)	855.6 (852.0, 853.3, 855.6) (59.8, 39, 1.2)	530.9 (528.9, 530.8) (61.6, 38.4)	73.8	700
9	B11	283.6	932.4 (932.2, 933.6) (89.3, 10.7)	855.8 (852.3, 853.7, 855.6) (56.7, 34.9, 8.4)	531.2 (529.3, 531.2) (95.4, 4.6)	74.4	700

[a] RT = reduction temperature.

to sample B11, suggesting that nickel is at different valence states as the amount of copper increases.[27] Third, the BE of the main peak was reduced on going from sample B1.8 to sample B11, as observed from curve-fitted values for samples 1, 2, and 3 in Table 3. The reduction in BE is thought to be attributed to the presence of copper in the reduced solid solution.

When Ni−Th alloys were studied by Fuggle and Zolnierek, the decrease in the BE of the main peak for Ni was related to an increase in nickel d hole density arising from filling them by adjacent electropositive thorium,[28] whereas for Ni−Pd alloys an increase in the BE of the main peak for Ni was observed, which was related to the reduction in nickel d hole density, namely, a charge transfer to adjacent electronegative palladium atoms from nickel.[29,30] In the case of Ni and Cu in this study, the reduction in the BEs for Ni also appears to be related to changes in unfilled d-band electron holes arising from the charge transfer from Cu to the adjacent Ni. Support for this hypothesis may also come from a previous study which showed that Ni catalytic activity decreased upon increasing copper content.[11] Further, the Ni $2p_{3/2}$ spectrum for sample B11 showed three curve-fitted values (sample 3 in Table 3), indicating that some of the Ni^{2+} ions were reduced at this level of copper doping, consistent with the shape change of the XPS spectrum for this sample. It should be noted that the shoulder on the low BE side of the main peak for sample B11 is solely due to reduction of Ni^{2+} ions, but its BE value (852.1 eV) is lower compared to that of bulk Ni (852.8 eV). The XRD peaks (Figure 3a) also showed the presence of Ni peaks in addition to NiO peaks for this sample reduced at 270 °C. Cu $2p_{3/2}$ curve-fitted BE values in Table 3 for samples 1, 2, and 3 also showed a decrease in the BEs from sample B1.8 to sample B11. Moreover, the Cu $2p_{3/2}$ curve-fitted values at lower BE for samples B3.5 and B11 (932.6 and 932.1 eV for samples 2 and 3, respectively) corresponded to Cu while the values at higher

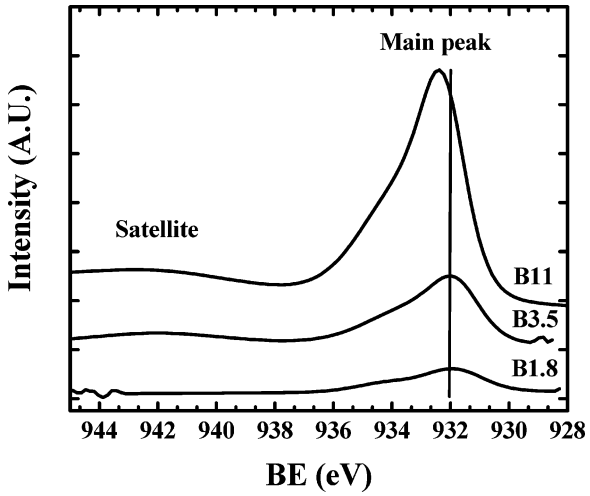

Figure 9. Cu $2p_{3/2}$ XPS spectra of samples B1.8, B3.8, and B11 reduced at 700 °C.

(27) Boske, T.; Maiti, K.; Knauff, O.; Ruck, K.; Golden, M. S.; Krabbes, G.; Fink, J.; Osafune, T.; Motoyama, N.; Eisaki, H.; Uchida, S. *Phys. Rev. B* **1998**, *57*, 138.
(28) Fuggle, J. C.; Zolnierek, Z. *Solid State Commun.* **1981**, *38*, 799.
(29) Kishi, K., Motoyoshi, Y.; Ikeda, S. *Surf. Sci.* **1981**, *105*, 313.
(30) Treglia, G.; Desjonqueres, M. C.; Duncastelle, F.; Spanjaad, D. *J. Phys.* **1981**, *C14*, 4347.

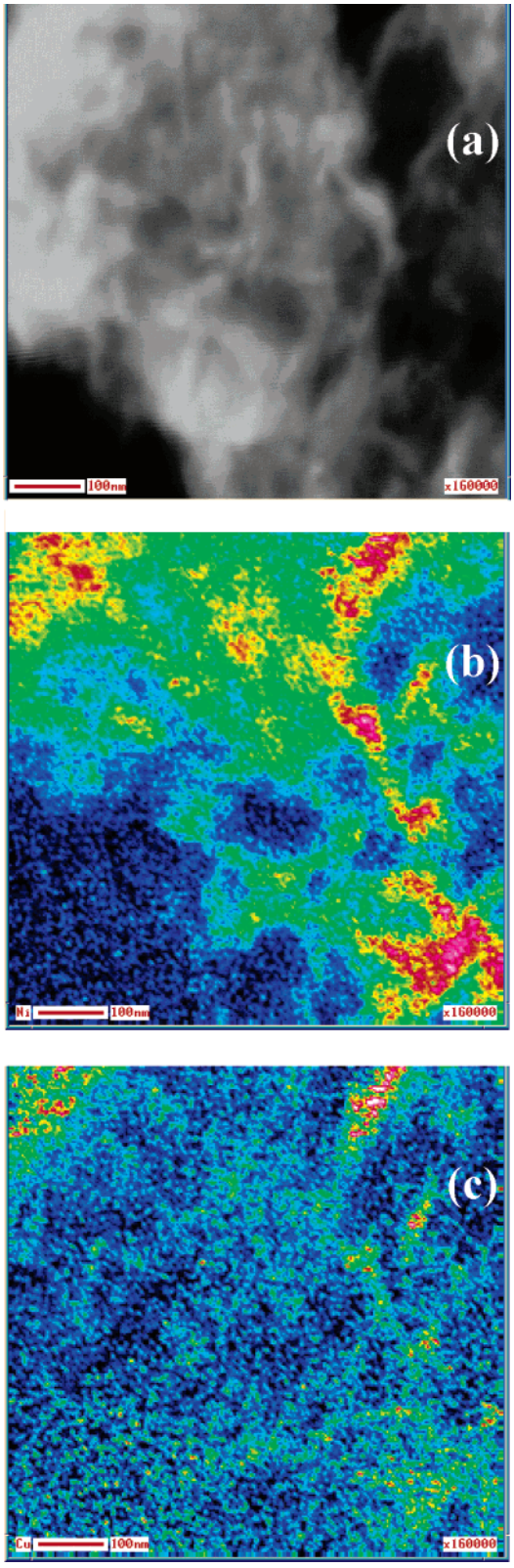

Figure 10. (a) SEM image, (b) Auger image of Ni, and (c) Auger image of copper for sample B1.8 reduced at 700 °C.

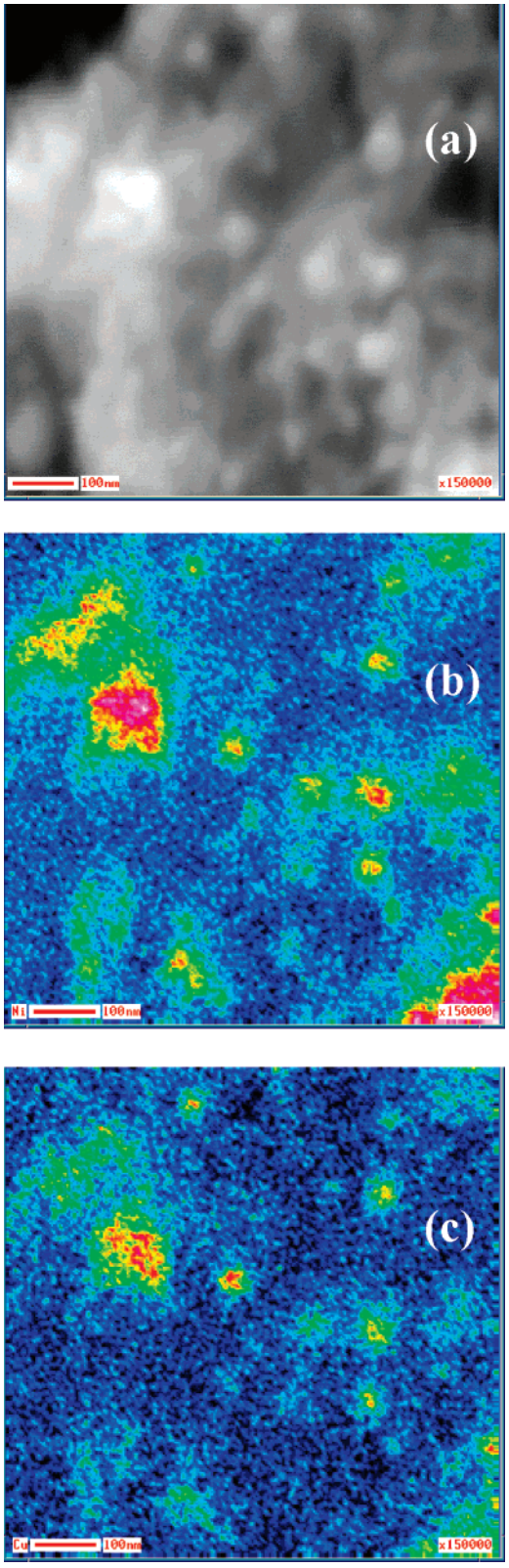

Figure 11. (a) SEM image, (b) Auger image of Ni, and (c) Auger image of copper for sample B11 reduced at 700 °C.

BE (933.8 and 933.5 eV, respectively) corresponded to Cu^{2+}, indicating that despite sample B1.8 some Cu^{2+} ions were reduced for samples B3.5 and B11 at 270 °C.

Figure 7 shows the Ni $2p_{3/2}$ XPS spectra for samples B1.8, B3.5, and B11 reduced at 450 °C. In general, it shows attributes similar to those observed for these samples in Figure 6. However, the presence of the shoulder on the low BE side of the main peak for sample B3.5 indicates that some Ni^{2+} ions were reduced at 450 °C for this sample in contrast to those at the reduction temperature of 270 °C. This is consistent with the curve-fitted BE value of sample 5 (852.4 eV) in Table 3 and XRD results in Figure 2b which showed

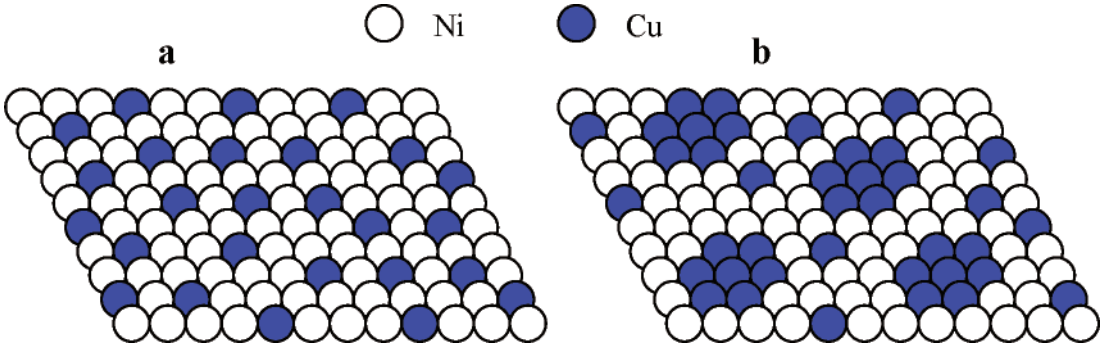

Figure 12. Proposed model for arrangements of nickel and copper atoms on the catalyst surface reduced at temperatures (a) below 700 °C and (b) around 700 °C.

the presence of the nickel phase in addition to NiO for sample B3.5 reduced at 450 °C. Moreover, the BE values, at the low BE side, were reduced on going from sample B3.5 to sample B11 by −0.3 eV (samples 5 and 6 in Table 3). The two other curve-fitted BE values at the high BE side for samples 5 and 6 represented Ni^{2+} ions of different neighboring atoms as previously discussed. Also, by inspection of the percentage of peak intensities of the curve-fitted BEs at the high BE side for samples 4, 5, and 6, it can be seen that the redistribution of Ni^{2+} ions occurred as the reduction temperature increased.

Figure 8 shows the Ni $2p_{3/2}$ XPS spectra for samples B1.8, B3.5, and B11 reduced at 700 °C. A shoulder corresponding to the reduction of Ni^{2+} ions appeared at the low BE side regardless of copper content, consistent with XRD profiles in Figure 3. For sample B1.8, the curve-fitted BE value, at the low BE side, was 852.1 eV while for sample B3.5 it was 852.0 eV. The most important observation in Figure 8 is the displacement of the BE shoulder for sample B11 to a higher value (852.3 eV) with respect to sample B3.5 (852.0 eV) which is inconsistent with the same samples reduced at 450 °C in Figure 7. This trend was also observed for the Cu $2p_{3/2}$ spectrum of sample B11 reduced at 700 °C shown in Figure 9 and Table 3 (sample 9). It is assumed that, at the reduction temperature of 700 °C, phase segregation of copper occurred for sample B11.

Auger Study. Figures 10 and 11 show SEM and Auger imaging of sample B1.8 and B11 reduced at 700 °C, respectively. The SEM images were taken from one small particle. In Auger imaging, hot colors, such as bright and red colors, represent a high concentration of the examined elements (copper and nickel) while cold colors, such as black and blue colors, represent a low concentration of the examined elements. By inspection of the Auger images of samples B1.8 and B11, it can be seen that the distribution of nickel and copper is not uniform in these samples. The Auger image of nickel for sample B1.8 in Figure 10b shows nickel clusters (bright and red colors), whereas the Auger image of copper in Figure 10c shows a more uniform distribution of copper (bright and red colors). Also, by comparison of the positions of the bright and red colors in Figures 10b and 10c, it can be seen that nickel and copper are located at about the same positions in Auger imaging. This indicates the possibility of forming alloyed Cu−Ni for this sample. For sample B11 in Figure 11, the Auger images of nickel and copper show that both nickel and copper are not as well-distributed as in sample B1.8. This can be appreciated by the scattered bright and red spots in Figures 11b and 11c. It is also interesting to note that, for sample B11, the copper and nickel atoms are at the exact positions in Figures 11b and 11c. Although their similar distribution cannot be predicted by Auger imaging, the XPS results previously shown predict a phase separation for this sample as is discussed below.

The discussion which was put forward for the nature of copper−nickel interactions and supported by XRD, XPS, and Auger imaging results helps us predict a model which represents what the actual surfaces of the alloy particles may look like under different reduction conditions. For this purpose, a model has been proposed for temperature-induced alloy segregation of nickel−copper alloys shown in Figure 12. According to this model, at temperatures above 700 °C where the interfacial energy is high, surface energies are minimized by copper and nickel segregation; hence, copper and nickel atoms tend to cluster rather than uniformly disperse on the support surface. This model is supported, first, from the observation of the changes of bonding energies for copper and nickel at these temperatures and, second, from the Auger imaging results which show a redistribution of these two metals at these temperatures.

Characterization of the chemical state of an element on a support by XPS has traditionally been carried out by comparing their BEs with those of bulk compounds. For example, for copper or copper oxide supported phases, BE changes have been attributed to the size of the deposited metals or oxides.[31,32] Several reasons for BE changes have also been invoked: variation of the average coordination number of particle atoms due to a high surface-to-volume ratio, decrease in the electron density of supported particles with respect to the bulk metal or oxide, and alloying and/or chemical interaction with the support. Similar changes in the electronic characteristics of oxide particles and layers deposited on substrates of other metal oxides were also attributed to the dispersion degree of the deposited phase (assuming this decreases with the amount of deposited material).[33,34] The results described herein show that changes in the BE values should be expected for Ni when it is in

(31) Rodriguez, N. M.; Kim, M. S.; Baker, T. K. *J. Catal*. **1993**, *140*, 16.
(32) Gonzalez-Elipe, A. R.; Munuera, G.; Espinos, J. P. *Surf. Interface Anal*. **1990**, *16*, 375.

solid solution with other elements, such as Al and Cu. The linking arrangements of nickel in the solid solution with other nickel or aluminum cations that were discussed accounted for the large changes in the BEs at the high end of the spectra. As described in the Experimental Section, the Ni−Cu alloy catalysts formed by reduction of homogeneous Ni−Cu−Al oxide solid solutions in hydrogen left behind an aluminum oxide support, in which nickel and copper adatoms become dispersed. It was also shown that when nickel was alloyed with copper, changes in the electronic properties of nickel resulted in displacement of BEs to lower values depending on the copper content. Changes in the electrical properties of nickel resulted in a change in its catalytic activity as was previously shown.[11]

A very thorough quantitative evaluation of each factor with respect to electronic variations between the Ni and Cu or Ni and Al and that for bulk nickel can be done by comparing the BE changes with the quantum mechanical bond structure of Ni−O−M (M: Al, Cu) at the interfaces.[34,35] However, this theoretical analysis is outside the scope of this paper because it aims at a phenomenological description of the alloy effects. Moreover, no structural information (i.e., coordination state and arrangement of the Cu, Ni, and Al atoms) is available at this stage to discuss these factors on a quantitative basis. This information and a quantum mechanical description of Ni−O−M bonds at the interfaces in terms of covalence and also the density of charge distribution would be necessary to completely account for the observed changes. Considered strictly on a qualitative basis, alloying nickel with copper increases the covalency of such a Ni−O bond, a factor that likely should contribute to a decrease in reduction temperature of nickel as well as shifting of the BE of Ni to lower values as were experimentally found in this study. For the reasons discussed above, it seems clear that preparation of alumina-supported Ni−Cu alloy catalysts described in previous work and characterized in this work may be superior to that of preparation methods using direct deposition (impregnation) of metal salts on a support such as alumina.

Conclusions

The XRD results of different copper−nickel−aluminum oxide solid solutions reduced at different temperatures showed that the metal phases that were formed upon reduction were sensitive to the copper content and reduction temperature. Analysis of metal phases and lattice parameter values showed that copper moderated the reduction temperature of nickel. Also, the BE values of nickel were sensitive to both the Ni−Ni arrangements in the solid solution and the amount of copper. The eventual effect of changes in the electronic properties of nickel upon alloying was a set of changes in the experimental BE values. A displacement of experimental nickel $2p_{3/2}$ BEs to higher values was found compared to bulk nickel. This was attributed to the Ni^{2+}−O−M (M: Ni^{2+}, Al^{3+}) bond structure in the solid solution. Although the presence of alumina was not detected in XRD profiles even at a reduction temperature of 700 °C, the experimental XPS BE values for aluminum corresponded well to that of Al^{3+}. When the curve-fitted BE values of nickel in the reduced oxide solid solutions were compared according to the copper doping, it was found that displacement of BE values depended on the copper content and the reduction temperature. At low copper doping and moderate temperatures, the nickel BEs decreased by the mechanism of charge transfer from copper to nickel. However, at high copper doping and at elevated reduction temperatures, the BEs tended to restore to those of bulk nickel due to copper segregation. Copper and nickel segregation were also observed in Auger imaging results of copper and nickel at reduction temperatures around 700 °C.

Acknowledgment. The financial support for the present work from the Alberta Energy Research Institute (AERI) under the COURSE research program is greatly appreciated.

CM051910O

(33) Jirka, I. *Surf. Sci*. **1990**, *232*, 307.
(34) Mejias, J. A.; Jimenez, V. M.; Lassaletta, G.; Fernandez, A.; Espinos, J. P.; Gonzalez-Elipe, A. R. *J. Phys. Chem*. **1996**, *100*, 16255.
(35) Barranco, A.; Yubero, F.; Mejias, J. A.; Espinos, J. P.; Gonzalez-Elipe, A. R. *Surf. Sci*. **2001**, *482*, 680.